This is a repository copy of *A Combined In Vitro/In Silico Approach to Identifying Off-Target Receptor Toxicity*.

Article

A Combined *In Vitro/In Silico* Approach to Identifying Off-Target Receptor Toxicity

Joseph Leedale,
Kieran J. Sharkey,
Helen E. Colley, ...,
Craig Murdoch,
Parveen Sharma,
Steven D. Webb

j.leedale@liverpool.ac.uk (J.L.)
psharma@liverpool.ac.uk (P.S.)

HIGHLIGHTS

Development of *in vitro/in silico* framework for identifying off-target toxicity

Mathematical modeling of receptor signaling and related transcriptional activity

Identification of key events in the signaling pathway

Off-target receptor activation *in vivo* simulated using PBPK modeling

Article

A Combined *In Vitro/In Silico* Approach to Identifying Off-Target Receptor Toxicity

Joseph Leedale,[1,6,*] Kieran J. Sharkey,[1] Helen E. Colley,[2] Áine M. Norton,[3] David Peeney,[3] Chantelle L. Mason,[4] Jean G. Sathish,[3,5] Craig Murdoch,[2] Parveen Sharma,[3,*] and Steven D. Webb[4]

SUMMARY

Many xenobiotics can bind to off-target receptors and cause toxicity via the dysregulation of downstream transcription factors. Identification of subsequent off-target toxicity in these chemicals has often required extensive chemical testing in animal models. An alternative, integrated *in vitro/in silico* approach for predicting toxic off-target functional responses is presented to refine *in vitro* receptor identification and reduce the burden on *in vivo* testing. As part of the methodology, mathematical modeling is used to mechanistically describe processes that regulate transcriptional activity following receptor-ligand binding informed by transcription factor signaling assays. Critical reactions in the signaling cascade are identified to highlight potential perturbation points in the biochemical network that can guide and optimize additional *in vitro* testing. A physiologically based pharmacokinetic model provides information on the timing and localization of different levels of receptor activation informing whole-body toxic potential resulting from off-target binding.

INTRODUCTION

Many drugs are designed to interact specifically with cell surface, cytoplasmic, or nuclear receptors to produce a beneficial therapeutic effect. However, drugs can often bind to and interact with receptors that are not their intended targets, and such "off-target" binding may cause what is now often termed a molecular initiating event (MIE), e.g., receptor activation of toxicological relevance that may ultimately lead to an adverse drug reaction (ADR) (Edwards and Aronson, 2000; Guengerich, 2011; Muller and Milton, 2012). In many instances, ADRs can lead to significant morbidity and mortality as well as contribute to high levels of attrition during drug development (Lazarou et al., 1998; Pirmohamed et al., 2004). This can primarily be attributed to an incomplete understanding of the molecular mechanism of action of a given compound and the lack of ability to predict which receptors may be activated unintentionally.

The sole use of *in vitro*-based experimental strategies in the early stages of drug development and chemical testing is important but can lead to an unreliable and incomplete understanding of reactions (Coleman, 2011). Therefore, often considerable numbers of animals are used to screen out chemicals that may cause off-target toxicity, with figures for the UK reporting that 306,000 *in vivo* toxicology safety procedures were performed in 2014 (Home Office, 2015). In addition, the chemical industry used almost 345,000 animals in the EU for toxicological or other safety evaluations (European Commission, 2013), and in the United States 3–6 million fish are used annually for whole effluent toxicity testing (Scholz et al., 2013). Furthermore, pharmacokinetics and pharmacodynamics are significantly different between animal models and humans, diminishing their effectiveness in detecting toxicity through pre-clinical studies (Lauschke et al., 2016). There is therefore a clear need to develop scientific approaches to identify toxicologically relevant off-target receptor binding to reduce the burden of animal use in toxicity testing. The development of a more ethical, non-animal toolkit for initial chemical toxicological assessment using an integrated human-based *in vitro/in silico* system would enhance current strategies and may even expedite the drug development pipeline.

In intracellular signaling, ligand/receptor interactions lead to the activation of a distinct set of transcription factors, the effects of which tend to be tissue specific. Several companies now offer transcription factor activation profiling platforms, and so it is possible to identify and catalog the transcription factor activation profiles of toxicologically relevant receptors upon binding of their known ligands/drugs. It is assumed that transcription factor profiles generated from off-target receptor activation of any given drug can be

[1]EPSRC Liverpool Centre for Mathematics in Healthcare, Department of Mathematical Sciences, University of Liverpool, Liverpool L69 7ZL, UK

[2]School of Clinical Dentistry, University of Sheffield, Sheffield S10 2TA, UK

[3]MRC Centre for Drug Safety Science, Department of Molecular and Clinical Pharmacology, University of Liverpool, Liverpool L69 3GE, UK

[4]Department of Applied Mathematics, Liverpool John Moores University, Liverpool L3 3AF, UK

[5]Immuno and Molecular Toxicology, Drug Safety Evaluation, Bristol-Myers Squibb, 1 Squibb Drive, New Brunswick, NJ 08903, USA

[6]Lead Contact

*Correspondence:
j.leedale@liverpool.ac.uk
(J.L.),
psharma@liverpool.ac.uk
(P.S.)

https://doi.org/10.1016/j.isci.2018.05.012

matched against known ligand/receptor transcription profiles to predict which specific receptor (or class of receptors) has been activated in the initial off-target MIE. However, when testing off-target profiles of new compounds, the resulting transcription profile may not precisely match that of a known receptor (e.g., partial agonism or the binding of multiple receptors), and therefore a method of refinement is required to narrow the subset of off-target receptors. Our approach aims to refine the *in vitro* receptor identification process for off-target receptors by using information about the changes in receptor-mediated transcription factor activity following the introduction of a given compound and integrating this information with predictive *in silico* models and analysis. This approach allows for the identification of relevant perturbations in the transcription factor signaling pathway that signify the binding of a receptor or smaller range of receptors as well as other points of interest in the transcription factor signaling network that can contribute toward and guide subsequent off-target receptor identification.

Translating the wealth of knowledge on network interactions of cellular components to dynamic models is generally limited by the amount of available quantitative information to accompany these relationships, such as molecular amounts and reaction rates. However, qualitative dynamic network modeling can be used to compare with routinely generated semi-quantitative experimental time course data, where perturbations can provide valuable information about the system. *In silico* modeling of this type then provides a platform for the refinement of more quantitative (parameter-based) modeling (Fisher et al., 2013). In such a scenario, the network modeling method of Petri nets provides an effective tool, particularly in the complex, stochastic framework of molecular biological pathways (Chaouiya, 2007; Heiner et al., 2008; Heidary et al., 2015). Petri nets are often used to model multiple species and reactions without defining large quantities of unknown parameters, as modeling emphasis is on network topology and relative amounts of species rather than on specific reaction rates. This emphasis on network structure can then be translated to methods such as flux balance analysis and metabolic control analysis (MCA) without knowledge of rate constants, as was shown for the switching of the metabolic pathway in *E. coli* (Edwards et al., 2001; Kitano, 2002).

The identification of off-target receptor binding alone for a given compound is insufficient to predict significant off-target toxicity, and so we aim to provide additional information to support and refine the subsequent evaluation of toxic potential. This is achieved by translating knowledge of receptor binding properties and relative distribution of the receptor throughout the body to a whole-body response to the xenobiotic. This approach utilizes a physiologically based pharmacokinetic (PBPK) model adapted specifically for describing receptor activation throughout the body following compound exposure. A PBPK model is a mechanistic, multi-compartment mathematical model that describes the time course dynamics and overall kinetics of an administered drug dose throughout the organism of interest. PBPK models integrate the physicochemical properties of the substance with the specific physiology of the organism such that the evolution of the ADME (absorption, distribution, metabolism, and excretion) processes can be simulated *in silico*. Drug/substance properties include tissue affinity, membrane permeability, enzymatic stability, etc., whereas the organism/system components include properties such as organ mass/volume and blood flow (Rowland et al., 2011). PBPK modeling is used in this work to couple the pharmacokinetics of a drug to dose-response parameters with the associated off-target receptor in different tissues to generate spatiotemporal dynamics of the off-target receptor activation.

RESULTS

Development of the Signaling Pathway Model

As proof of concept, an *in silico* model of the histamine H1 receptor signaling pathway was formulated. This pathway was chosen owing to the well-understood intracellular signaling interactions involved upon receptor stimulation and the existence of a known off-target partial agonist, lisuride (Bakker et al., 2004). The H1 receptor is a G-protein-coupled receptor that, upon activation, leads to dissociation of $G\alpha_{q/11}$ and the $G\beta\gamma$ complex. $G\alpha_{q/11}$ activates phospholipase Cβ (PLCβ), leading to hydrolysis of phosphatidylinositol 4,5-biphosphate (PIP$_2$) and the formation of inositol triphosphate (IP$_3$) and diacylglycerol (DAG) (Bakker et al., 2001; Sandal et al., 2013). IP$_3$ mediates a transient intracellular calcium release from the ER (Shah et al., 2015) that eventually mediates the activation of nuclear factor of activated T-cells (NFAT) (Macian, 2005), cAMP response element-binding protein (CREB) (Johannessen and Moens, 2007), and myocyte enhancer factor-2 (Mef2) transcription factors (Lu et al., 2000). DAG simultaneously activates protein kinase C (PKC), and this phosphorylates IκB kinase (IKK), ultimately leading to nuclear factor kappa-light-chain-enhancer of activated B cells (NF-κB) transcription factor activation (La Porta and Comolli, 1997). The $G\beta\gamma$ complex also plays a role in histamine signal transduction, regulating many effectors,

Transcription Factor	Fold Change in Relative Luciferase Units
NFAT	1.97 ± 0.063
NF-κB	2.18 ± 1.47
CREB	1.54 ± 0.027
MEF2	2.74 ± 1.31
ATF2	1.67 ± 8.99

**Table 1. Transcription Factor Changes**

Alterations in expression levels of specified genes in the presence of histamine after 6 hr expressed as mean fold changes in relative luciferase units with SD(n = 3) as determined by Cignal reporter assay.

including adenylate cyclase (AC) (Maruko et al., 2005) and phosphoinositide 3 kinase (PI3K) (Gautam et al., 1998). AC mediates the subsequent activation of protein kinase A via cyclic AMP (cAMP) leading to CREB phosphorylation and transcription factor activation (Mosenden and Taskén, 2011). PI3K mediates the activation of Akt, NF-κB, and activating transcription factor 2 (ATF2) (Bence et al., 1997; Breitwieser et al., 2007). To provide semi-quantitative information for the relative transcription factor dynamics as described earlier, we assayed pathway perturbations using a luciferase reporter-based transcription factor array to calibrate the fold increase expected of key signaling outputs upon stimulation with an agonist. These transcription factors were identified as NFAT, NF-κB, CREB, Mef2, and ATF2. Incubation of H1 receptor-expressing HeLa cells with histamine showed considerable activation of these transcription factors (Table 1).

A stochastic Petri net model of the histamine H1 receptor signaling pathway was formulated based on existing knowledge of the pathway and network interactions with the five critical transcription factors determined to be activated following ligand binding. The pathway in this proof of concept provides an illustrative example of what should ultimately form part of a larger cell signaling model that incorporates the complexity of the known toxicological receptors and associated transcription factors in the proposed methodology. The H1 Petri net includes the key dynamic molecular species and appropriate network interactions that are activated during ligand-binding-induced signaling. This pathway is depicted using the modified Edinburgh pathway notation (mEPN) format (Freeman et al., 2010) in Figure 1 and directly corresponds to the layout of the Petri net. All rates are equal such that all stochastic transitions are equally likely to fire but are effectively modulated by the concentration of upstream reactants in a mass action process. Time is interpreted qualitatively reflecting the relative order of events. Varying quantities in the mathematical model, such as the amount of ligand introduced ("dose") and the total amounts of system species (i.e., moieties of active and inactive states for each protein), modulate the scale of transcriptional activity regulation, and as such, these values were optimized to correlate with the experimental signaling assays. This optimization was carried out by assuming a large-scale continuum approximation of the Petri net to a system of ordinary differential equations (ODEs) and fitting to the corresponding transcription factor output data (Figure 2). It should be noted that the optimal parameter set is non-identifiable for such a large system with relatively few data points to fit. However, this issue was the precise motivation for the combined Petri net/MCA approach, which is well suited to understanding the relative impact of small perturbations on the transcription factors of interest and prioritize network connectivity information in favor of accurate predictions of parameters and dynamics (Koch et al., 2010). Corresponding pathway reactions, moieties, and ODEs can be found in the supplementary material. In addition to providing static information on the network interactions of the signaling pathway and relative changes in steady state activity following receptor activation, Petri nets can also be used to simulate transient temporal dynamics, providing further dynamic information on the relative order and scale of transcriptional regulation (Figure 3) following a receptor-ligand binding event. However, it is clear that more data would be required for one to relate this dynamic output to the biological context and validate any potential predictions about transient dynamics.

Analysis of Network Perturbations to Identify Off-Target Responses

The identification of significant pathway reactions upstream of transcription was achieved using metabolic control analysis (MCA), which is a mathematical technique that tests the sensitivity of a given variable to network perturbations (Kacser and Burns, 1973; Heinrich and Rapoport, 1974). Specifically, scaled MCA
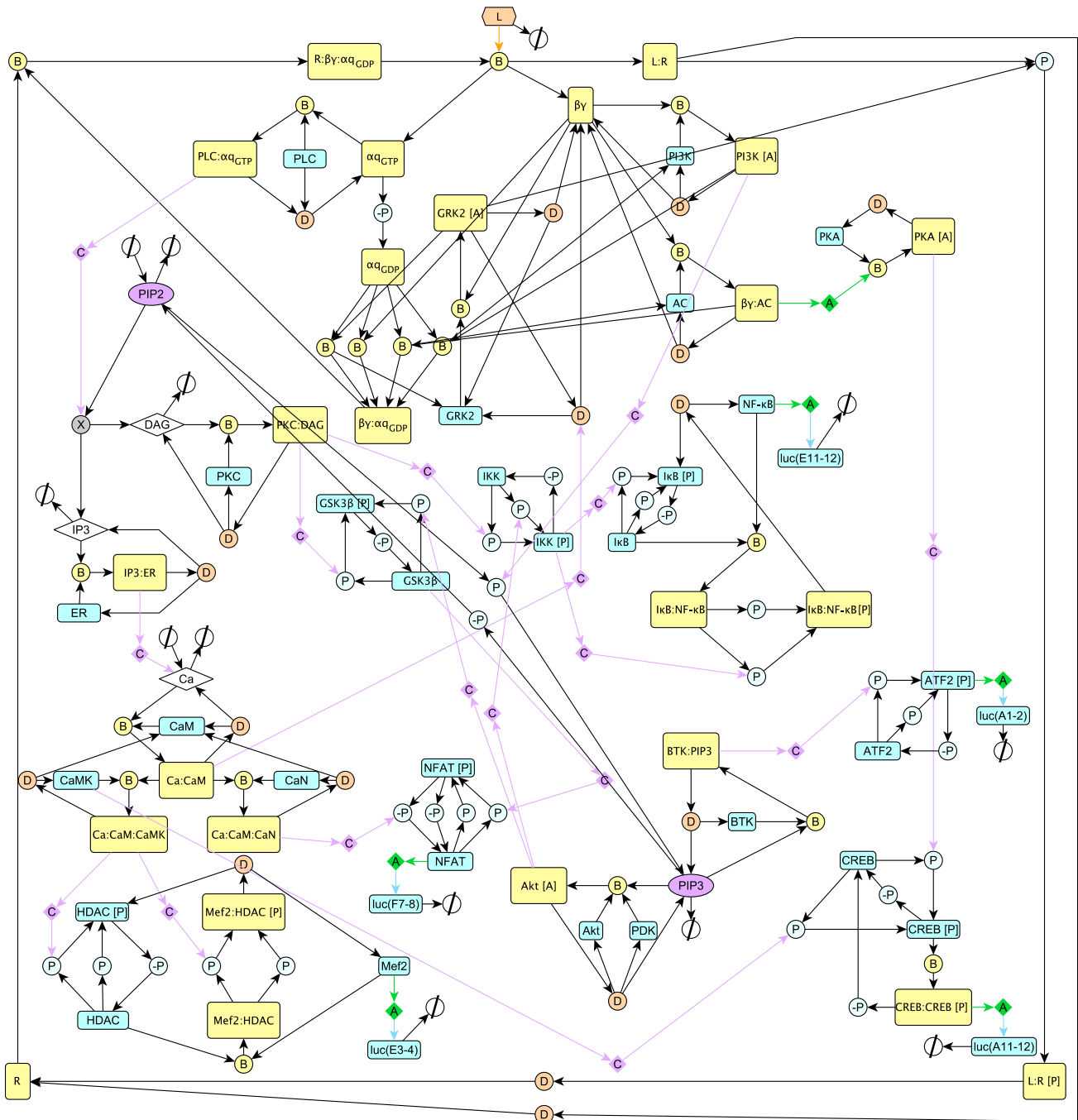
Figure 1. Schematic Representation for the Petri Net of the Histamine H1 Receptor Signaling Pathway Using mEPN Notation

The Petri net describes the key relationships between components of the signaling pathway system culminating in the regulation of downstream transcription factor expression stimulated by the binding of a ligand to the histamine H1 receptor.

concentration control coefficients provide the ratio between a relative measure of change in the steady state of a system variable as affected by perturbations in network reaction rates. In our illustrative H1 example model, MCA coefficients were calculated for each transcription factor that was experimentally determined to show significant change in activity following binding of the H1 receptor (Figure 4). The rows of the heatmap in Figure 4 correspond to the numbered reactions as indicated in the supplementary material. MCA points not only to the direct regulation of gene transcription as critical to H1-associated
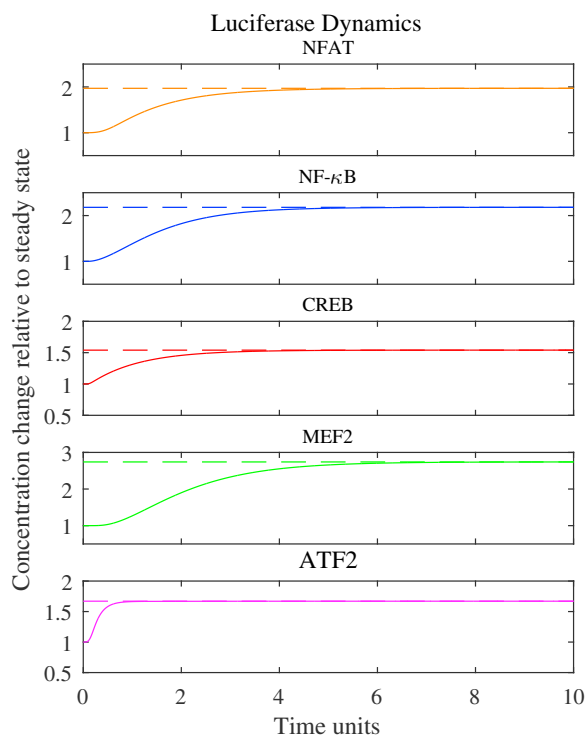
Figure 2. Optimized Transcription Factor Output

The ligand (histamine) was introduced at t = 0 (Petri net time units) in the model simulation. Before t = 0 the model was run to steady state. The model solution was fit to the data via optimization of the conserved moieties of the signaling pathway. Dotted lines represent the fold increase in transcriptional activity for the relevant transcription factor observed in the transcription assays. Solid lines represent the normalized model solution for the corresponding transcriptional activity as simulated by luciferase dynamics.

transcriptional activity (white patches in Figure 4), but also to other reactions within the cascade, upstream of the transcription factors and downstream of the target receptor. For example, in this system the transcriptional activity of Mef2 is sensitive to relatively distant biochemical reactions, such as the rate of calcium release from the ER (24% of maximum sensitivity provided by perturbation of Mef2 transcription rate). Also, the model suggests that the transcriptional activity of ATF2 is more sensitive to perturbations in PIP2 synthesis than to the regulation of the BTK:PIP3 complex that directly activates ATF2 by phosphorylation.

The identification of these sensitive perturbation points within the signaling pathway model provide information beyond the transcription factor activity measurements found experimentally, which allows for more optimized, directed experimental designs for receptor identification, if initial screening fails to identify the off-target receptor. For example, for a given compound that was shown to regulate Mef2 transcriptional activity but did not interact with the H1 receptor, this model would inform a proposal to screen for receptors that are known to interact with biochemical reactions identified as being sensitive, such as calcium release, during MCA.

Translation to Tissue Scales Using a PBPK Model

Following an *in silico* identification of an off-target receptor, extrapolation to the study of potential *in vivo* toxicity can be performed using a PBPK model. For our illustrative example, receptor binding properties are provided by EC_{50} dose-response curves for the off-target H1 agonist, lisuride (Figure 5A), and measurements of the corresponding binding affinity, K_d (Bakker et al., 2004). The dose-response curves were estimated by fitting the following equation to the dose-response data:

$$Response\% = Min + \frac{(Max - Min)L^n}{EC_{50}^n + L^n},$$ (Equation 1)
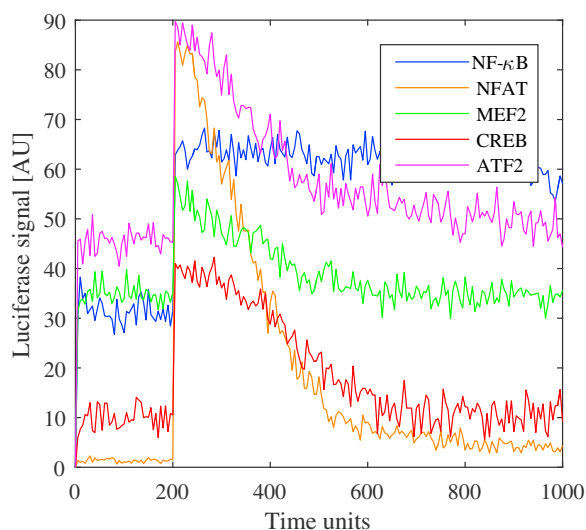
Figure 3. Transient Dynamic Output of the Histamine H1 Receptor Signaling Pathway Using the Stochastic Petri Net

This figure illustrates the dynamic output of the stochastic Petri net when a small transient perturbation to the ligand concentration is made at t = 200 units, representing the pre-stimulation steady state. Dynamics are shown for model variables that correspond to luciferase signals for transcription factors associated with a receptor stimulation perturbation.

for ligand concentration L. The optimized parameter values are given in Table 2. To provide tissue-specific responses we also used western blot measurements of relative H1 receptor expression in different tissues (Figures 5B and 5C) and calculated modified tissue-specific EC_{50} values using

$$EC_{50_i} = \frac{K_d EC_{50}}{R_i(K_d + EC_{50}) - EC_{50}}$$

where i denotes the ith tissue, K_d is the dissociation equilibrium constant for lisuride, and R_i is a measure of receptor abundancy in tissue i (see Table 3). For simplicity, this model assumes that the same amount of receptor binding is required to achieve 50% response in each tissue in the absence of any other information, particularly as the response measured is proximal to receptor binding attenuating any potential amplification effects arising from potential signaling cascades in different tissues (Kenakin, 2009). For further information regarding this derivation see the Supplemental Information.

To simulate the pharmacokinetics of lisuride throughout the body, physicochemical properties of the compound were required, which were obtained from previously published measurements. These properties include lipophilicity, whether the drug is neutral/acid/base, solubility (obtained from the DrugBank database [Wishart et al., 2006]), molecular weight (O'Neil, 2013), acid dissociation constant (Meloun et al., 2005), and effective permeability (Winiwarter et al., 1998). The time course dynamics simulated by the PBPK model for drug concentration in each tissue compartment of the body were then coupled to receptor binding properties and relative receptor expression in tissues to provide a predictive temporal response throughout the body. This response can be produced for any dosage regimen and various methods of administration, such as intravenous, oral, and inhalation. The PBPK model was based on the form derived by Peters (2008). The model was optimized for lisuride physicochemical and binding properties and the H1 receptor distribution throughout the different tissues. Example lisuride response kinetics following both intravenous (IV) and oral administrations can be found in Figure 6. The IV dose of 25 μg/mL used in Figure 6 was the same as that used in a previous pharmacokinetic study for relevance (Krause et al., 1991). These experimental data were also the IV data used to optimize the PBPK model to recapitulate the lisuride dynamics in the venous blood compartment and also simulate corresponding oral profiles as per the methodology described by Peters (2008). The oral dose of 0.1 mg chosen for the PBPK model was deemed relevant by matching previous pharmacological studies (Koizumi et al., 1985; Al-Sereiti and Turner, 1989). The dynamic response of the H1 receptor is visualized over time as a solution to Equation (1)
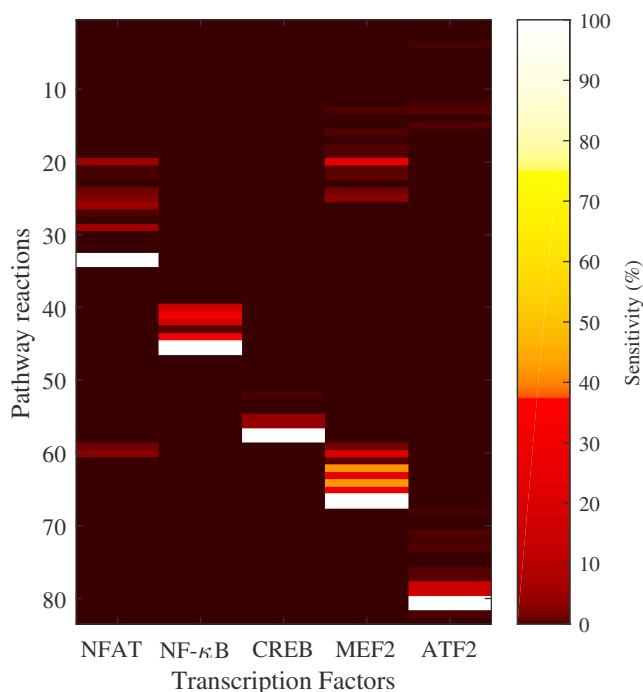
Figure 4. Metabolic Control Analysis (MCA) of the H1 Signaling Pathway

Scaled concentration control coefficients as a result of MCA are plotted for the activity of five transcription factors modulated by histamine H1 receptor binding. Each row of the heatmap numerically corresponds to a reaction term in the signaling pathway model (see Supplemental Information). Maximum and minimum values in the heatmap (white patches) represent maximum sensitivity to perturbation of the reaction terms in the model depicting direct transcriptional regulation rates and luciferase decay rates.

with tissue-specific EC_{50} values for the pharmacokinetics of lisuride (*L*) in different parts of the body. Both IV and oral administration simulations are plotted to also highlight the impact of delivery route. This is particularly pertinent in this case where we are studying a receptor that has a relatively high concentration in the gastrointestinal tract. IV administration results in relatively high receptor stimulation in the liver, brain, small intestine, and colon at earlier times, whereas oral administration results in a more gradual accumulation in these tissues and the receptors in the colon are stimulated at a near-maximal level for a relatively long time after oral ingestion. These simulations allow us to compare how the off-target response varies throughout the body over time depending on the pharmacokinetics of the drug coupled with physiologically relevant receptor availability and receptor binding information. Such information is potentially useful to determine whether or not an identified off-target agonist is likely to elicit an off-target receptor response in an area of high target density based on its physicochemical properties.

DISCUSSION

ADRs are a major cause of patient morbidity, mortality, and drug attrition during development (Pirmohamed et al., 2004). This can be attributed to a poor understanding of the mechanisms underlying the toxic response and also to a lack of current tools for the prediction of a toxic outcome. Animal models have a limited scope, and data obtained using such models may not be ideal for ascertaining toxicity seen in humans. As such, computational systems biology models can be essential tools to improve chemical reaction predictivity (Krewski et al., 2010). In this study, we describe a new *in silico* modeling method that can be used to enhance the current knowledge of pathway perturbations to provide a new toxicity-testing paradigm based on human biology. In this method, chemical-mediated activation of transcription factors and intracellular signaling pathway molecules were used as readouts to inform and drive a pathway-based *in silico* approach to identify possible upstream receptor(s) engaged by such chemicals. *In vitro* data were then used to inform a PBPK *in silico* modeling platform to understand and rank the risk of toxicity at tissue, organ, and whole-body levels over time. Key to this integrative approach was the coupling of *in vitro* experimental techniques and advanced *in silico* modeling to create a unique resource that, with further
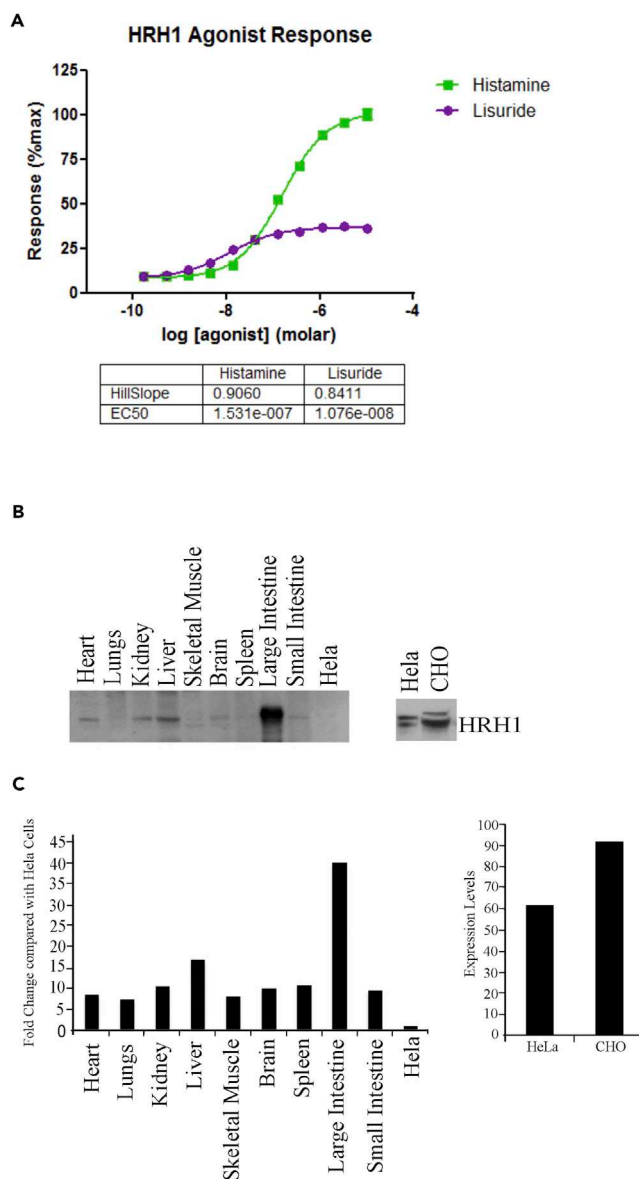
Figure 5. Histamine/Lisuride Dose Response, EC$_{50}$, and Kinetic Parameters

(A) Ligand (histamine) and partial agonist (lisuride) dose-response assays used to calculate EC$_{50}$ values.

(B) Immunoblotting of H1 receptor in murine organs.

(C) Relative quantification of immunoblot relative to HeLa cell lysates.

development and parameterization, could be used to predict the off-target toxicity of compounds that can then inform and direct more focused *in vivo* experimentation.

Mathematical modeling was used to mechanistically describe the processes that lead to regulation of transcriptional activity following the binding of ligand to receptor. This was achieved by designing a signaling pathway model that represented all the relevant processes and biochemical reactions downstream of ligand binding, culminating in the regulation of transcription. We have established a novel *in vitro/in silico* approach using data from assays measuring transcription factor activation and chemically induced perturbations of intracellular signaling pathways to inform *in silico* pathway modeling. This unbiased pathway-led approach uses computational simulations to identify causality between receptor activation and pathway perturbations to aid identification of the upstream receptor/s engaged by the initial MIE. As proof of concept, an *in silico* Petri net model of the histamine H1 receptor-signaling pathway was formulated

Parameter	Value	SE	Units
Min	7.98%	1.066	/
Max	36.55%	0.5863	/
$logEC_{50}$	−7.968	0.06724	mol/L
n (Hill coefficient)	0.8411	0.1009	/
K_d	8×10^{-9}	0.0577	mol/L

Table 2. Kinetic Parameters of Lisuride and the Histamine H1 Receptor
Receptor activation of the H1 histamine receptor was studied with known agonist (histamine) and off-target agonist (lisuride). Using these assays, each parameter was calculated using GraphPad Prism.

with the off-target compound, lisuride. The output of this system provides semi-quantitative temporal dynamics for the entire pathway that can be used to investigate system perturbations, simulate experiments, and provide structural pathway predictions. *In vitro* reporter assay data were then used to parameterize and validate the model, and the identification of critical candidate perturbation points was achieved using MCA. Signaling pathway models can be purposely used in this methodology to provide a library of MCA coefficients for a range of transcription factors associated with receptor binding and toxicity and guide further experimentation. In the example shown, calcium release from the ER and PIP2 synthesis are highlighted as important upstream events for the transcriptional activity of Mef2 and ATF2. If a new compound is shown to induce the activity of these transcription factors but the receptor responsible is not identified via screening, for instance, further testing could be guided toward targets that modulate these upstream processes. This illustrates the feasibility of this approach in directing further experimentation toward relevant pathway mechanisms or receptor clusters during the process of receptor identification via focused *in vitro* assay testing.

In vitro to *in vivo* extrapolations of whole-body consequences of receptor binding was explored using PBPK modeling. The structure of PBPK models typically revolves around the anatomical structure of the organism, with different organs and tissues of varying perfusion rates being separated into distinct compartments. These compartments are then coupled through the circulation, whose arterial and venous flow is described to connect the organs in a physiological way. Entrance points (e.g., absorption) of the model depend on the drug administration method (e.g., inhalation, ingestion, injection), whereas exit points (e.g., excretion) are generally described via the kidneys and intestine. The flow kinetics of the model determine distribution, whereas metabolism occurs in the liver and intestine. The inherent physiological basis distinguishes true PBPK models from their PK model counterparts that usually simplify the physiology to fewer hypothetical compartments of different flow rates, driven by the data/process of interest, such that they are often more tractable analytically. In contrast, PBPK models are generally more complex but are designed to have a better global representation such that valid extrapolations can be made and disparate experimental data can be integrated during model parameterization. In this way, PBPK models are less reliant on data fitting to obtain appropriate values for equation parameters and essentially the same model (with appropriate modifications) can be suitably applied in many different pharmacological scenarios for quantitative risk assessment and therapy optimization.

PBPK model simulations are increasingly being used in pharmacology, in both academia and industry, to provide important predictions of the pharmacokinetic properties and toxic potential of new drugs at an early stage in drug development (Zhao et al., 2011; Jones and Rowland-Yeo, 2013; Tsamandouras et al., 2015). This type of *in silico* testing can offer a quicker, cheaper, and more ethical alternative method when compared with traditional *in vivo* experiments performed. Ideally, both experimental and computational methods are used harmoniously to provide a cycle of information and enhanced knowledge iteration as the accuracy of PBPK models inevitably rely on quality experimental data to calibrate rates within the differential equations. In the method reported here, physicochemical properties of the chemical are combined with tissue-specific receptor expression and EC_{50} data to predict time course dynamics of the chemical concentrations in each tissue, as well as tissue-level receptor-activation responses to that chemical. These predictions can be produced for any dosage regimen and various methods of administration. In the example study of the off-target partial agonist of the histamine H1 receptor, lisuride, the combination of lisuride pharmacokinetics and relative H1 receptor distribution throughout the body allowed us

Parameter	Value	Tissue
R_{HE}	5.60	Heart
R_{LU}	3.56	Lungs
R_{KI}	6.64	Kidney
R_{LI}	11.63	Liver
R_{BO}	3.88	Skeletal muscle
R_{BR}	5.78	Brain
R_{SP}	5.83	Spleen
R_{SI}	5.56	Small intestine
R_{CO}	25.90	Large intestine

Table 3. Relative Amounts of Histamine H1 Receptor in Murine Tissue Calculated Using Immunoblot Analysis

Values were used to calculate tissue-specific receptor scaling factors for lisuride EC_{50} values when binding to the histamine H1 receptor.

to predict that the dose response would be most significant in the brain, liver, and gastrointestinal system. In this case example, these results are supported by prior knowledge of the compound and receptor, although the modeling was done agnostic of such prior *in vivo* findings. In particular, receptor response localized to the brain is somewhat expected since lisuride is primarily a psychotherapeutic drug, affecting dopamine and serotonin regulation (Marona-Lewicka et al., 2002). Lisuride is primarily metabolized in the liver, where there is a relatively high expression of histamine receptors. There is also high receptor expression in the gastrointestinal tract owing to the role of histamine in intestinal secretion and motility (Leurs et al., 1995; Sander et al., 2006). Furthermore, lisuride administration in patients with Parkinson disease has been associated with gastrointestinal side effects (Ebadi and Pfeiffer, 2004). Although relative response rates have been quantified by the model in different parts of the body at different times, to translate what such a response directly represents in the context of toxicity and clinical relevance is very complicated, and restricted in this methodology, establishing a challenge beyond the scope of this paper. However, these PBPK-based extrapolations do allow us to generate predictive data relevant to risk assessment and further translation to toxicity at the organ and whole-body levels for off-target receptor perturbations. The output provided by this method is intended to identify toxic potential and guide subsequent *in vitro* and *in vivo* experimentation to organs of interest/importance.

The operating parameters of the approach are circumscribed by the extent of current knowledge regarding receptors and their function. This represents a potential limitation of the strategy, although the mathematically driven signaling pathway model has the potential to identify novel, uncharacterized receptor targets. The challenge of identifying sensitive perturbation points within large-scale networks of receptor signaling pathways required that a semi-quantitative network-based approach be used. This inevitably limits the amount of predictive, dynamic information that can be extrapolated, and caution must be exercised such that the utility of mathematical models is preserved by acknowledging the relevant application that stimulated its design. The approach is experimental (with elements of modeling and extrapolation to assess and rank toxicological risk) and does not incorporate prediction of receptor binding based on chemical or receptor structures. The strength of the methodology is predicated on currently available, validated experimental methods, as it does not require the development of new, untested technologies and relies on sound criteria-based selection of receptors and quantifying receptor function and binding using established experimental techniques. Future work requires the development of multiple pathway models based on training chemical data as well as the integration of pathways, which should be optimized and validated with non-training data. Furthermore, the current PBPK framework can be extended to ensure improved predictive potential by incorporating mechanistic tissue models, catering for a wider range of chemicals and capturing population-level responses. More work is also needed to translate tissue-level receptor activation responses to measures of toxicity, such as relevant biomarkers. Carefully calculated person-to-person variation and covariances within organism-related parameters would also allow for the prediction of a population response whereby different individuals within a sample population may exhibit different levels of exposure and therefore associated toxicity from the same dosage levels. The combined *in vitro/in silico*
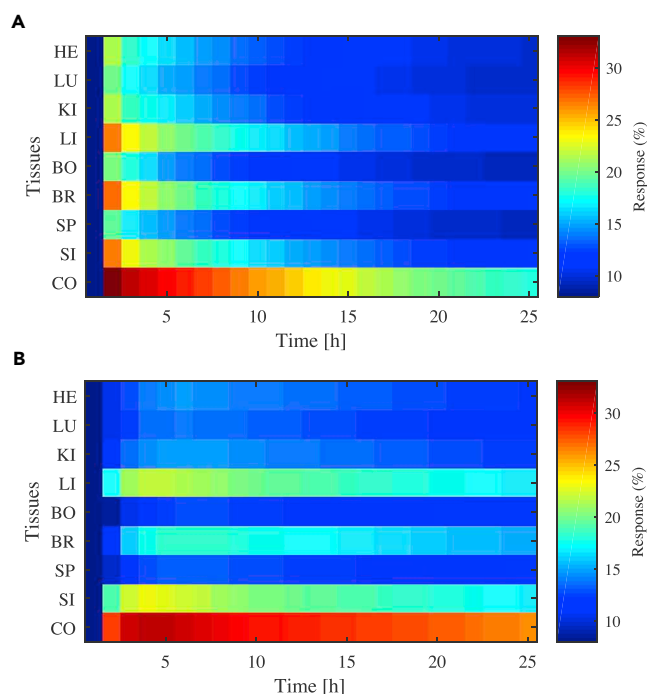
Figure 6. Temporal Tissue Response Predicted by PBPK Modeling Following Doses of Lisuride

(A) 25 μg/mL administered intravenously.

(B) 0.1 mg administered orally. Tissues are labeled as follows: heart (HE), lungs (LU), kidneys (KI), liver (LI), bone (BO), brain (BR), spleen (SP), small intestine (SI), and colon (CO).

approach of this study has shown how the multidisciplinary, iterative process of systems biology can be applied to direct experiments, optimize the utility of generated data, and challenge and refine theoretical modeling to improve methods for detecting and predicting toxicity caused by compounds that bind to off-target receptors.

METHODS

All methods can be found in the accompanying Transparent Methods supplemental file.

SUPPLEMENTAL INFORMATION

Supplemental Information includes Transparent Methods, two figures, and four tables and can be found with this article online at https://doi.org/10.1016/j.isci.2018.05.012.

ACKNOWLEDGMENTS

AUTHOR CONTRIBUTIONS

J.L. contributed to the mathematical modeling and wrote the manuscript; K.J.S. and C.L.M. contributed to the mathematical modeling; H.E.C. and C.M. contributed to the design of the experimental work; A.M.N. and D.P. performed the experiments; J.G.S. designed the research; P.S. contributed to, designed, and per-formed the experimental work; S.D.W. contributed to the mathematical modeling and directed the research. All authors read and approved the final manuscript.

DECLARATION OF INTERESTS

The authors declare no competing interests.

iScience

CellPress

REFERENCES

Al-Sereiti, M.R., and Turner, P. (1989). The effects of lisuride, terguride and bromocriptine on intraocular pressure (IOP). Br. J. Clin. Pharmacol. 27, 159–163.

Bakker, R.A., Schoonus, S.B.J., Smit, M.J., Timmerman, H., and Leurs, R. (2001). Histamine H1-receptor activation of nuclear factor-κB: roles for Gβγ-and Gαq/11-subunits in constitutive and agonist-mediated signaling. Mol. Pharmacol. 60, 1133–1142.

Bakker, R.A., Weiner, D.M., Ter Laak, T., Beuming, T., Zuiderveld, O.P., Edelbroek, M., Hacksell, U., Timmerman, H., Brann, M.R., and Leurs, R. (2004). 8R-lisuride is a potent stereospecific histamine H1-receptor partial agonist. Mol. Pharmacol. 65, 538–549.

Bence, K., Ma, W., Kozasa, T., and Huang, X.-Y. (1997). Direct stimulation of Bruton's tyrosine kinase by Gq-protein α-subunit. Nature 389, 296–299.

Breitwieser, W., Lyons, S., Flenniken, A.M., Ashton, G., Bruder, G., Willington, M., Lacaud, G., Kouskoff, V., and Jones, N. (2007). Feedback regulation of p38 activity via ATF2 is essential for survival of embryonic liver cells. Genes Dev. 21, 2069–2082.

Chaouiya, C. (2007). Petri net modelling of biological networks. Brief. Bioinform. 8, 210–219.

Coleman, R.A. (2011). Human tissue in the evaluation of safety and efficacy of new medicines: a viable alternative to animal models? ISRN Pharm. 2011, 806789.

Ebadi, M., and Pfeiffer, R.F. (2004). Parkinson's Disease (CRC Press).

Edwards, I.R., and Aronson, J.K. (2000). Adverse drug reactions: definitions, diagnosis, and management. Lancet 356, 1255–1259.

Edwards, J.S., Ibarra, R.U., and Palsson, B.O. (2001). In silico predictions of Escherichia coli metabolic capabilities are consistent with experimental data. Nat. Biotechnol. 19, 125–130.

European Commission (2013). Seventh report on the statistics on the number of animals used for experimental and other scientific purposes in the member states of the European union. Available at: http://eur-lex.europa.eu/resource.html?uri=cellar:e99d2a56-32fc-4f60-ad69-61ead7e377e8.0001.03/DOC_1&format=PDF.

Fisher, C.P., Plant, N.J., Moore, J.B., and Kierzek, A.M. (2013). QSSPN: dynamic simulation of molecular interaction networks describing gene regulation, signalling and whole-cell metabolism in human cells. Bioinformatics 29, 3181–3190.

Freeman, T.C., Raza, S., Theocharidis, A., and Ghazal, P. (2010). The mEPN scheme: an intuitive and flexible graphical system for rendering biological pathways. BMC Syst. Biol. 4, 65.

Gautam, N., Downes, G.B., Yan, K., and Kisselev, O. (1998). The G-protein βγ complex. Cell. Signal. 10, 447–455.

Guengerich, F.P. (2011). Mechanisms of drug toxicity and relevance to pharmaceutical development. Drug Metab. Pharmacokinet. 26, 3–14.

Heidary, Z., Ghaisari, J., Moein, S., Naderi, M., and Gheisari, Y. (2015). Stochastic Petri net modeling of hypoxia pathway predicts a novel incoherent feed-forward loop controlling SDF-1 expression in acute kidney injury. IEEE Trans. Nanobioscience 15, 19–26.

Heiner, M., Gilbert, D., and Donaldson, R. (2008). Petri Nets for Systems and Synthetic Biology. Formal Methods for Computational Systems Biology (Springer), pp. 215–264.

Heinrich, R., and Rapoport, T.A. (1974). A linear steady-state treatment of enzymatic chains. FEBS J. 42, 97–105.

Home Office (2015). Annual statistics of scientific procedures on living animals Great Britain 2014. Available at: https://assets.publishing.service.gov.uk/government/uploads/system/uploads/attachment_data/file/469508/spanimals14.pdf.

Johannessen, M., and Moens, U. (2007). Multisite phosphorylation of the cAMP response element-binding protein (CREB) by a diversity of protein kinases. Front. Biosci. 12, e32.

Jones, H.M., and Rowland-Yeo, K. (2013). Basic concepts in physiologically based pharmacokinetic modeling in drug discovery and development. CPT Pharmacometrics Syst. Pharmacol. 2, 1–12.

Kacser, H., and Burns, J.A. (1973). The control of flux. Symp. Soc. Exp. Biol. 27, 65–104.

Kenakin, T. (2009). A Pharmacology Primer: Theory, Application and Methods (Academic Press).

Kitano, H. (2002). Systems biology: a brief overview. Science 295, 1662–1664.

Koch, I., Reisig, W., and Schreiber, F. (2010). Modeling in Systems Biology: The Petri Net Approach (Springer Science & Business Media).

Koizumi, K., Aono, T., and Kurachi, K. (1985). The effect of lisuride hydrogen maleate on anterior pituitary hormones, oestradiol and cortisol in normal and hyperprolactinaemic women. Eur. J. Obstetrics Gynecol. Reprod. Biol. 20, 19–26.

Krause, W., Mager, T., Kühne, G., Duka, T., and Voet, B. (1991). The pharmacokinetics and pharmacodynamics of lisuride in healthy volunteers after intravenous, intramuscular, and subcutaneous injection. Eur. J. Clin. Pharmacol. 40, 399–403.

Krewski, D., Acosta, D., Jr., Andersen, M., Anderson, H., Bailar, J.C., III, Boekelheide, K., Brent, R., Charnley, G., Cheung, V.G., and Green, S., Jr. (2010). Toxicity testing in the 21st century: a vision and a strategy. J. Toxicol. Environ. Health B Crit. Rev. 13, 51–138.

La Porta, C.A., and Comolli, R. (1997). PKC-dependent modulation of IkB alpha-NFkB pathway in low metastatic B16F1 murine melanoma cells and in highly metastatic BL6 cells. Anticancer Res. 18, 2591–2597.

Lauschke, V.M., Hendriks, D.F.G., Bell, C.C., Andersson, T.B., and Ingelman-Sundberg, M. (2016). Novel 3D culture systems for studies of human liver function and assessments of the hepatotoxicity of drugs and drug candidates. Chem. Res. Toxicol. 29, 1936–1955.

Lazarou, J., Pomeranz, B.H., and Corey, P.N. (1998). Incidence of adverse drug reactions in hospitalized patients: a meta-analysis of prospective studies. JAMA 279, 1200–1205.

Leurs, R., Smit, M., and Timmerman, H. (1995). Molecular pharmacological aspects of histamine receptors. Pharmacol. Ther. 66, 413–463.

Lu, J., McKinsey, T.A., Nicol, R.L., and Olson, E.N. (2000). Signal-dependent activation of the MEF2 transcription factor by dissociation from histone deacetylases. Proc. Natl. Acad. Sci. USA 97, 4070–4075.

Macian, F. (2005). NFAT proteins: key regulators of T-cell development and function. Nat. Rev. Immunol. 5, 472–484.

Marona-Lewicka, D., Kurrasch-Orbaugh, D.M., Selken, J.R., Cumbay, M.G., Lisnicchia, J.G., and Nichols, D.E. (2002). Re-evaluation of lisuride pharmacology: 5-hydroxytryptamine1A receptor-mediated behavioral effects overlap its other properties in rats. Psychopharmacology 164, 93–107.

Maruko, T., Nakahara, T., Sakamoto, K., Saito, M., Sugimoto, N., Takuwa, Y., and Ishii, K. (2005). Involvement of the βγ subunits of G proteins in the cAMP response induced by stimulation of the histamine H1 receptor. Naunyn Schmiedebergs Arch. Pharmacol. 372, 153–159.

Meloun, M., Syrovy, T., and Vrana, A. (2005). The thermodynamic dissociation constants of haemanthamine, lisuride, metergoline and nicergoline by the regression analysis of spectrophotometric data. Anal. Chim. Acta 543, 254–266.

Mosenden, R., and Taskén, K. (2011). Cyclic AMP-mediated immune regulation—overview of mechanisms of action in T cells. Cell. Signal. 23, 1009–1016.

Muller, P.Y., and Milton, M.N. (2012). The determination and interpretation of the therapeutic index in drug development. Nat. Rev. Drug Discov. *11*, 751–761.

O'Neil, M.J. (2013). The Merck Index: An Encyclopedia of Chemicals, Drugs, and Biologicals (Royal Society of Chemistry).

Peters, S.A. (2008). Evaluation of a generic physiologically based pharmacokinetic model for lineshape analysis. Clin. Pharmacokinet. *47*, 261–275.

Pirmohamed, M., James, S., Meakin, S., Green, C., Scott, A.K., Walley, T.J., Farrar, K., Park, B.K., and Breckenridge, A.M. (2004). Adverse drug reactions as cause of admission to hospital: prospective analysis of 18 820 patients. BMJ *329*, 15–19.

Rowland, M., Peck, C., and Tucker, G. (2011). Physiologically-based pharmacokinetics in drug development and regulatory science. Annu. Rev. Pharmacol. Toxicol. *51*, 45–73.

Sandal, M., Paltrinieri, D., Carloni, P., Musiani, F., and Giorgetti, A. (2013). Structure/function relationships of phospholipases C Beta. Curr. Protein Pept. Sci. *14*, 650–657.

Sander, L.E., Lorentz, A., Sellge, G., Coeffier, M., Neipp, M., Veres, T., Frieling, T., Meier, P.N., Manns, M.P., and Bischoff, S.C. (2006). Selective expression of histamine receptors H1R, H2R, and H4R, but not H3R, in the human intestinal tract. Gut *55*, 498–504.

Scholz, S., Sela, E., Blaha, L., Braunbeck, T., Galay-Burgos, M., Garcia-Franco, M., Guinea, J., Kluever, N., Schirmer, K., and Tanneberger, K. (2013). A European perspective on alternatives to animal testing for environmental hazard identification and risk assessment. Regul. Toxicol. Pharmacol. *67*, 506–530.

Shah, S.Z.A., Zhao, D., Khan, S.H., and Yang, L. (2015). Regulatory mechanisms of endoplasmic reticulum resident IP3 receptors. J. Mol. Neurosci. *56*, 938–948.

Tsamandouras, N., Rostami-Hodjegan, A., and Aarons, L. (2015). Combining the 'bottom up' and 'top down' approaches in pharmacokinetic modelling: fitting PBPK models to observed clinical data. Br. J. Clin. Pharmacol. *79*, 48–55.

Winiwarter, S., Bonham, N.M., Ax, F., Hallberg, A., Lennernäs, H., and Karlén, A. (1998). Correlation of human jejunal permeability (in vivo) of drugs with experimentally and theoretically derived parameters. A multivariate data analysis approach. J. Med. Chem. *41*, 4939–4949.

Wishart, D.S., Knox, C., Guo, A.C., Shrivastava, S., Hassanali, M., Stothard, P., Chang, Z., and Woolsey, J. (2006). DrugBank: a comprehensive resource for in silico drug discovery and exploration. Nucleic Acids Res. *34*, D668–D672.

Zhao, P., Zhang, L., Grillo, J.A., Liu, Q., Bullock, J.M., Moon, Y.J., Song, P., Brar, S.S., Madabushi, R., and Wu, T.C. (2011). Applications of physiologically based pharmacokinetic (PBPK) modeling and simulation during regulatory review. Clin. Pharmacol. Ther. *89*, 259–267.

Supplemental Information

A Combined *In Vitro*/*In Silico*

Approach to Identifying

Off-Target Receptor Toxicity

Joseph Leedale, Kieran J. Sharkey, Helen E. Colley, Áine M. Norton, David Peeney, Chantelle L. Mason, Jean G. Sathish, Craig Murdoch, Parveen Sharma, and Steven D. Webb

Supplementary Material

Transparent Methods

Experimental Methods

Cell culture

HeLa cells were cultured in Dulbecco's Modified Eagle Medium supplemented with 10% foetal bovine serum, 2 mM glutamine and incubated at 37 °C in a 5% CO_2 humidified atmosphere.

Quantification of transcription factor activation

Transcription factor activation was measured using Cignal Reporter dual-luciferase assay (Qiagen) as per manufacturer's instructions, to determine intracellular signal transduction perturbation and transcription factor activation data for *in silico* modelling. Briefly, HeLa cells were plated in 96-well plates and transfected with inducible transcription factor responsive constructs composed of specific transcription factor response elements linked to firefly luciferase along with a constitutively expressing *Renilla* construct as an internal control. Transfection was performed with Attractene transfection reagent (Qiagen) as per manufacturer's instructions. Transfected cells were stimulated with histamine (Sigma) for 6 or 24 h and activation of specific transcription factors quantified by luminometer using the Dual-Luciferase Reporter Assay System (Promega).

Receptor activation

Activation of histamine receptor H1 with its known agonist, histamine and the off-target partial agonist, lisuride was determined using PathHunter® Chinese Hamster Overy (CHO)-K1 reporter cells that over-express ProLink™-tagged human histamine H1 receptor and the Enzyme Acceptor (EA)-tagged β-Arrestin (DiscoverX) as per manufacturer's instructions. In these cells activation of histamine receptor H1 by a ligand forces H1 receptor coupling with EA-tagged β-Arrestin leading to the formation of a functional enzyme that is able to generate a chemiluminescent signal upon substrate cleavage. These assays were used to calculate EC50 values for both histamine and lisuride.

Immunoblotting analysis

Mouse organs from wild type C57 mice (Charles River) were snap frozen in liquid nitrogen and whole tissue lysates homogenised in lysis buffer (250 mM sucrose, 50 mM Tris.HCl,1 mM $MgCl_2$, 1% Triton X-100, 1 mM PMSF). Lysates were also generated from HeLa and CHO cells over-expressing histamine H1 receptor. The lysates were centrifuged at 5000 g for 15 minutes at 4 °C and 20 μg of total protein separated using SDS-PAGE and analysed using standard immunoblotting techniques. Membranes were blocked overnight in 5% milk powder in blocking buffer (0.2% Triton X-100 in PBS) at 4 °C and then incubated with rabbit polyclonal anti-H_1R antiserum (Abcam; 1:1000) followed by horseradish peroxidase-conjugated goat anti-rabbit antiserum (Jackson Labs; 1:2500). Immuno-reactive proteins were

visualized using enhanced chemiluminescent substrate detection (ThermoFisher). Densitometry analysis was carried out using Image J and fold-changes in expression relative to HeLa cells calculated.

Petri Nets

The stochastic Petri net model of the histamine H1 receptor signalling pathway was formulated using Snoopy software (Heiner et al., 2012). In the context of cellular signalling pathways, a Petri net is a bipartite graphical representation of a biochemical network with "tokens"/dots-or-numbers (representing number of molecules or concentration) in "places"/circles (network species, proteins etc.). A reaction is represented by the "firing" of a "transition"/square where tokens are moved from one place to a downstream place as indicated by connecting "arcs"/arrows. A transition may fire only if all upstream places contain sufficient tokens, i.e. all reactants must be present for a specific reaction to occur. Petri nets use mass action and Gillespie algorithm principles such that transitions with a higher number of upstream tokens fire with a higher probability.

Parameter Optimisation and Metabolic Control Analysis

The signalling pathway model large-scale continuum approximation to an ODE system was solved using a Runge-Kutta 4/5th order method with Matlab R2015b software. Pathway moieties (conserved quantities defined in supplementary material S1.2) were optimised such that model signalling output was consistent with experimental data. Optimisation was carried out by minimising the error between fold-increase in transcription factor levels in the model and the data. Metabolic scaled concentration control coefficients were calculated using Copasi 4.15 software (Hoops et al., 2006). The Peters (2008) PBPK model code was written and solved with Matlab R2015b software.

1 Modelling the H1 receptor signalling pathway

Table S1, related to Figure 1: Histamine H1 receptor signalling pathway reactions. Each reaction in the Petri net of Figure 1 is described explicitly with associated description and mass action kinetics.

Reaction No.	Reaction	Description	Mass action flux terms
1.	$L + R{:}\beta\gamma{:}\alpha q_{GDP} \rightarrow L{:}R + \beta\gamma + \alpha q_{GTP}$	Ligand binding causes dissociation of αq_{GTP} (i.e. GTP bound αq) and $\beta\gamma$ from the receptor	$v_1 = L * R{:}\beta\gamma{:}\alpha q_{GDP}$
2.	$GRK2 + \beta\gamma \rightarrow GRK2^*$	Activation of G protein coupled receptor kinase 2 ($GRK2$) by binding to free $\beta\gamma$	$v_2 = GRK2 * \beta\gamma$
3.	$GRK2 + \beta\gamma \xleftarrow{\;CaM{:}Ca+background\;} GRK2^*$	$CaM{:}Ca$ (defined below) mediated plus background deactivation of $GRK2$	$v_3 = GRK2^* * CaM{:}Ca + GRK2^*$
4.	$\alpha q_{GTP} \rightarrow \alpha q_{GDP}$	Background hydrolysis of αq_{GTP} to αq_{GDP}	$v_4 = \alpha q_{GTP}$
5.	$\alpha q_{GDP} + GRK2^* \rightarrow GRK2 + \beta\gamma{:}\alpha q_{GDP}$	αq_{GDP} will scavenge $\beta\gamma$ from complexes to give a $\beta\gamma{:}\alpha q_{GDP}$ complex	$v_5 = \alpha q_{GDP} * GRK2^*$
6.	$L{:}R \xrightarrow{\;GRK2^*\;} pL{:}R$	$GRK2^*$ phosphorylates agonist-activated receptors	$v_6 = L{:}R * GRK2^*$
7.	$pL{:}R \rightarrow R$	The phosphorylated receptors are recognized by arrestins that bind to the receptor which targets it for internalization	$v_7 = pL{:}R$
8.	$L{:}R \rightarrow R$	Background degradation of ligand	$v_8 = L{:}R$

Reaction No.	Reaction	Description	Mass action flux terms
9.	$\beta\gamma + \alpha q_{GDP} \rightarrow \beta\gamma{:}\alpha q_{GDP}$	αq_{GDP} binding with free $\beta\gamma$	$v_9 = \beta\gamma * \alpha q_{GDP}$
10.	$\beta\gamma{:}\alpha q_{GDP} + R \rightarrow R{:}\beta\gamma{:}\alpha q_{GDP}$	Binding of $\beta\gamma{:}\alpha q_{GDP}$ to free receptor to give $R{:}\beta\gamma{:}\alpha q_{GDP}$	$v_{10} = \beta\gamma{:}\alpha q_{GDP} * R$
11.	$\alpha q_{GTP} + PLC \rightarrow PLC{:}\alpha q_{GTP}$	PLC and αq_{GTP} binding	$v_{11} = \alpha q_{GTP} * PLC$
12.	$PLC{:}\alpha q_{GTP} \rightarrow PLC + \alpha q_{GDP}$	Dissociation of $PLC{:}\alpha q_{GTP}$ hydrolyses αq_{GTP} to αq_{GDP}	$v_{12} = PLC{:}\alpha q_{GTP}$
13.	$\emptyset \rightarrow PIP2$	Background production/synthesis	$v_{13} = k_1$
14.	$PIP2 \rightarrow \emptyset$	Background decay/utilisation	$v_{14} = PIP2$
15.	$PIP2 \xrightarrow{PLC:\alpha q_{GTP}} IP3 + DAG$	$PLC{:}\alpha q_{GTP}$ catalysed separation of $PIP2$ into $IP3$ and DAG	$v_{15} = PIP2 * PLC{:}\alpha q_{GTP}$
16.	$IP3 \rightarrow \emptyset$	Background decay/utilisation	$v_{16} = IP3$
17.	$DAG \rightarrow \emptyset$	Background decay/utilisation	$v_{17} = DAG$
18.	$IP3 + ER \rightarrow IP3{:}ER$	$IP3$ binding to receptors on the ER (endoplasmic reticulum)	$v_{18} = IP3 * ER$
19.	$IP3 + ER \leftarrow IP3{:}ER$	$IP3{:}ER$ dissociation	$v_{19} = IP3{:}ER$
20.	$\emptyset \xrightarrow{IP3:ER+background} Ca$	$IP3{:}ER$ induces Calcium (Ca) release from the ER. Plus background release/production	$v_{20} = IP3{:}ER + k_2$
21.	$Ca \rightarrow \emptyset$	Ca is sequestered back in to ER	$v_{21} = Ca$

Reaction No.	Reaction	Description	Mass action flux terms
22.			
23.	$Ca + CaM \rightarrow CaM{:}Ca$	Ca binds with Calmodulin (CaM).	$v_{22} = Ca * CaM$
24.	$Ca + CaM \leftarrow CaM{:}Ca$	$CaM{:}Ca$ dissociation	$v_{23} = CaM{:}Ca$
25.	$CaM{:}Ca + CaN \rightarrow CaM{:}Ca{:}CaN$	$CaM{:}Ca$ binds to Calcineurin (CaN).	$v_{24} = CaM{:}Ca * CaN$
26.	$CaM + CaN \leftarrow CaM{:}Ca{:}CaN$	$CaM{:}Ca{:}CaN$ dissociation	$v_{25} = CaM{:}Ca{:}CaN$
27.	$pNFAT \xrightarrow{CaM:Ca:CaN} NFAT$	$CaM{:}Ca{:}CaN$ induced dephosphorylation of $pNFAT$	$v_{26} = pNFAT * CaM{:}Ca{:}CaN$
28.	$pNFAT \rightarrow NFAT$	(background) dephosphorylation of $pNFAT$	$v_{27} = pNFAT$
29.	$NFAT \xrightarrow{GSK3\beta} pNFAT$	$pNFAT$ = inactive $NFAT$ (no signal)	$v_{28} = GSK3\beta * NFAT$
30.	$NFAT \rightarrow pNFAT$	(background) phosphorylation of $NFAT$	$v_{29} = NFAT$
31.	$GSK3\beta \xrightarrow{PKC:DAG} pGSK3\beta$	$PKC{:}DAG$ catalysed phosphorylation of glycogen synthase kinase 3 beta ($GSK3\beta$)	$v_{30} = GSK3\beta * PKC{:}DAG$
32.	$GSK3\beta \xrightarrow{Akt^*} pGSK3\beta$	Akt^* catalysed phosphorylation of $GSK3\beta$	$v_{31} = GSK3\beta * Akt^*$
33.	$GSK3\beta \leftarrow pGSK3\beta$	Dephosphorylation	$v_{32} = pGSK3\beta$
34.	$\emptyset \xrightarrow{NFAT} luc(\text{F7}-8)$	Luciferase F7-8 signal	$v_{33} = NFAT$
35.	$luc(\text{F7}-8) \rightarrow \emptyset$	Decay of luciferase signal	$v_{34} = luc(\text{F7}-8)$
36.	$PKC + DAG \rightarrow PKC{:}DAG$	Binding	$v_{35} = PKC * DAG$
37.	$PKC + DAG \leftarrow PKC{:}DAG$	Dissociation	$v_{36} = PKC{:}DAG$

Reaction No.	Reaction	Description	Mass action flux terms
38.			
39.	$IKK \xrightarrow{PKC:DAG} IKKp$	$PKC:DAG$ catalysed phosphorylation of IKK	$v_{37} = IKK * PKC:DAG$
40.	$IKK \xrightarrow{Akt^*} IKKp$	Akt^* catalysed phosphorylation of IKK	$v_{38} = IKK * Akt^*$
41.	$IKK \leftarrow IKKp$	Dephosphorylation	$v_{39} = IKKp$
42.	$I\kappa B \xrightarrow{IKKp+background} pI\kappa B$	$IKKp$ catalysed phosphorylation of $I\kappa B$.	$v_{40} = I\kappa B * IKKp + I\kappa B$
43.	$I\kappa B \leftarrow pI\kappa B$	Dephosphorylation	$v_{41} = pI\kappa B$
44.	$NF\kappa B + I\kappa B \rightarrow I\kappa B:NF\kappa B$	Binding	$v_{42} = NF\kappa B * I\kappa B$
45.	$I\kappa B:NF\kappa B \xrightarrow{IKKp+background} pI\kappa B:NF\kappa B$	$IKKp$ catalysed phosphorylation of $I\kappa B$	$v_{43} = I\kappa B:NF\kappa B * IKKp$ $+ I\kappa B:NF\kappa B$
46.	$pI\kappa B:NF\kappa B \rightarrow pI\kappa B + NF\kappa B$	Dissociation	$v_{44} = pI\kappa B:NF\kappa B$
47.	$\emptyset \xrightarrow{NFKB} luc(E11-12)$	Luciferase E11-12 signal	$v_{45} = NF\kappa B$
48.	$luc(E11-12) \rightarrow \emptyset$	Decay of luciferase signal	$v_{46} = luc(E11-12)$
49.	$\beta\gamma + AC \rightarrow \beta\gamma:AC$	Binding of Adenylyl Cyclase (AC, an enzyme) to $\beta\gamma$	$v_{47} = \beta\gamma * AC$
50.	$\beta\gamma + AC \leftarrow \beta\gamma:AC$	Dissociation	$v_{48} = \beta\gamma:AC$
51.	$\alpha q_{GDP} + \beta\gamma:AC \rightarrow AC + \beta\gamma:\alpha q_{GDP}$	αq_{GDP} will scavenge $\beta\gamma$ from complexes to give a $\beta\gamma:\alpha q_{GDP}$ complex	$v_{49} = \alpha q_{GDP} * \beta\gamma:AC$
52.	$PKA \xrightarrow{\beta\gamma:AC} PKA^*$	Activation of Protein Kinase A (PKA)	$v_{50} = PKA * \beta\gamma:AC$

Reaction No.	Reaction	Description	Mass action flux terms
53.			
54.	$PKA \leftarrow PKA^*$	Dissociation	$v_{51} = PKA^*$
55.	$CREB \xrightarrow{PKA^*} pCREB$	PKA^* catalysed phosphorylation of $CREB$	$v_{52} = CREB * PKA^*$
56.	$CREB \xrightarrow{CaM:Ca:CaMK} pCREB$	$CaM:Ca:CaMK$ (defined below) catalysed phosphorylation of $CREB$	$v_{53} = CREB * CaM:Ca:CaMK$
57.	$CREB \leftarrow pCREB$	Dephosphorylation	$v_{54} = pCREB$
58.	$pCREB + pCREB \rightarrow pCREB:pCREB$	Homerdimer formation	$v_{55} = pCREB * pCREB$
59.	$CREB + CREB \leftarrow pCREB:pCREB$	Dissociation	$v_{56} = pCREB:pCREB$
60.	$\emptyset \xrightarrow{pCREB:pCREB} luc(\text{A11} - 12)$	Luciferase A11-12 signal	$v_{57} = pCREB:pCREB$
61.	$luc(\text{A11} - 12) \rightarrow \emptyset$	Decay of luciferase signal	$v_{58} = luc(\text{A11} - 12)$
62.	$CaM:Ca + CaMK \rightarrow CaM:Ca:CaMK$	$CaM:Ca$ binding reversibly to CaM kinases ($CaMK$).	$v_{59} = CaM:Ca * CaMK$
63.	$CaM + CaMK \leftarrow CaM:Ca:CaMK$	Dissociation	$v_{60} = CaM:Ca:CaMK$
64.	$Mef2:HDAC \xrightarrow{CaM:Ca:CaMK+background} Mef2:pHDAC$	$CaM:Ca:CaMK$ catalysed + background phosphorylation of $HDAC$ within the $Mef2:HDAC$ complex.	$v_{61} = Mef2:HDAC$ $* CaM:Ca:CaMK$ $+ Mef2:HDAC$
65.	$Mef2:pHDAC \rightarrow Mef2 + pHDAC$	Dissociation	$v_{62} = Mef2:pHDAC$

Reaction No.	Reaction	Description	Mass action flux terms
66.			
67.	$HDAC \xrightarrow{CaM:Ca:CaMK+background} pHDAC$	$CaM:Ca:CaMK$ catalysed + background phosphorylation of free $HDAC$	$v_{63} = HDAC * CaM:Ca:CaMK + HDAC$
68.	$pHDAC \rightarrow HDAC$	Background dephosphorylation	$v_{64} = pHDAC$
69.	$Mef2 + HDAC \rightarrow Mef2:HDAC$	Binding of myocyte enhancer factor-2 ($Mef2$) to $HDAC$.	$v_{65} = HDAC * Mef2$
70.	$\emptyset \xrightarrow{Mef2} luc(E3-4)$	Luciferase E3-4 signal	$v_{66} = Mef2$
71.	$luc(E3-4) \rightarrow \emptyset$	Decay of luciferase signal	$v_{67} = luc(E3-4)$
72.	$\beta\gamma + PI3K \rightarrow PI3K^*$	Binding to give active phosphoinositol-3-kinase ($PI3K^*$).	$v_{68} = \beta\gamma * PI3K$
73.	$\beta\gamma + PI3K \leftarrow PI3K^*$	Dissociation	$v_{69} = PI3K^*$
74.	$\alpha q_{GDP} + PI3K^* \rightarrow PI3K + \beta\gamma:\alpha q_{GDP}$	αq_{GDP} will scavenge $\beta\gamma$ from complexes to give a $\beta\gamma:\alpha q_{GDP}$ complex.	$v_{70} = \alpha q_{GDP} * PI3K^*$
75.	$PIP2 \xrightarrow{PI3K^*} PIP3$	$PI3K^*$ catalysed production of inositol lipid $PIP3$ from $PIP2$	$v_{71} = PIP2 * PI3K^*$
76.	$PIP3 \rightarrow PIP2$	Catalysed by PTEN (assumed constant)	$v_{72} = PIP3$
77.	$PIP3 \rightarrow \emptyset$	Background decay/utilisation	$v_{73} = PIP3$
78.	$PIP3 + Akt + PDK \rightarrow Akt^*$	Activation of Akt.	$v_{74} = PIP3 * Akt * PDK$
79.	$PIP3 + Akt + PDK \leftarrow Akt^*$	Dissociation	$v_{75} = Akt^*$

Reaction No.	Reaction	Description	Mass action flux terms
80.			
81.	$BTK + PIP3 \rightarrow BTK{:}PIP3$	Reversible binding of $PIP3$ with Bruton's tyrosine kinase (BTK).	$v_{76} = BTK * PIP3$
82.	$BTK + PIP3 \leftarrow BTK{:}PIP3$	Dissociation	$v_{77} = BTK{:}PIP3$
83.	$ATF2 \xrightarrow{BTK:PIP3+background} pATF2$	$BTK{:}PIP3$ catalysed phosphorylation of activating transcription factor 2 ($ATF2$).	$v_{78} = ATF2 * BTK{:}PIP3 + ATF2$
84.	$ATF2 \leftarrow pATF2$	Dephosphorylation	$v_{79} = pATF2$
85.	$\emptyset \xrightarrow{pATF2} luc(\text{A1} - 2)$	Luciferase A1-2 signal	$v_{80} = pATF2$
86.	$luc(A1 - 2) \rightarrow \emptyset$	Decay of luciferase signal	$v_{81} = luc(A1 - 2)$
87.	$\emptyset \leftrightarrow L$	Basal degradation of ligand (and basal synthesis during infusion simulations)	$v_{82} = k_3 - L$

Table S2, related to Figure 1: List of pathway moieties. Each equation represents a fixed total amount based on a sum of related variables.

1	$\beta\gamma_{total} = \beta\gamma + R{:}\beta\gamma{:}\alpha q_{GDP} + \beta\gamma{:}\alpha q_{GDP} + \beta\gamma{:}AC + PI3K^* + GRK2^*$	14	$NF\kappa B_{total} = NF\kappa B + I\kappa B{:}NF\kappa B + pI\kappa B{:}NF\kappa B$
2	$R_{total} = R + L{:}R + pL{:}R + R{:}\beta\gamma{:}\alpha q_{GDP}$	15	$AC_{total} = AC + \beta\gamma{:}AC$
3	$\alpha q_{total} = \alpha q_{GTP} + \alpha q_{GDP} + PLC{:}\alpha q_{GTP} + R{:}\beta\gamma{:}\alpha q_{GDP} + \beta\gamma{:}\alpha q_{GDP} = \beta\gamma_{total}$	16	$PKA_{total} = PKA + PKA^*$
4	$GRK2_{total} = GRK2 + GRK2^*$	17	$CREB_{total} = CREB + pCREB + 2pCREB{:}pCREB$
5	$PLC_{total} = PLC + PLC{:}\alpha q_{GTP}$	18	$CaMK_{total} = CaMK + CaM{:}Ca{:}CaMK$
6	$ER_{total} = ER + IP3{:}ER$	19	$HDAC_{total} = HDAC + pHDAC + Mef2{:}HDAC + Mef2{:}pHDAC$
7	$CaM_{total} = CaM + CaM{:}Ca + CaM{:}Ca{:}CN + CaM{:}Ca{:}CaMK$	20	$Mef2_{total} = Mef2 + Mef2{:}HDAC + Mef2{:}pHDAC$
8	$CN_{total} = CN + CaM{:}Ca{:}CN$	21	$PI3K_{total} = PI3K + PI3K^*$
9	$NFAT_{total} = NFAT + pNFAT$	22	$Akt_{total} = Akt + Akt^*$
10	$GSK3\beta_{total} = GSK3\beta + pGSK3\beta$	23	$PDK_{total} = PDK + Akt^*$
11	$PKC_{total} = PKC + PKC{:}DAG$	24	$BTK_{total} = BTK + BTK{:}PIP3$
12	$IKK_{total} = IKK + IKKp$	25	$ATF2_{total} = ATF2 + pATF2$
13	$I\kappa B_{total} = I\kappa B + pI\kappa B + I\kappa B{:}NF\kappa B + pI\kappa B{:}NF\kappa B$		

Table S3, related to Figure 2: Pathway model ODEs (large-scale continuum approximation). The systems of ODEs representing the histamine H1 receptor signaling pathway are provided below. $d[i]/dt$ represents the rate of change of variable i over time, t. Note that reaction $v(j)$ corresponds to reaction j in Table S1.

Ordinary Differential Equations
$\dfrac{d[L]}{dt} = v(82) - v(1)$
$\dfrac{d[\beta\gamma]}{dt} = v(1) + v(3) + v(48) + v(69) - v(2) - v(9) - v(47) - v(68)$
$\dfrac{d[L:R]}{dt} = v(1) - v(6) - v(8)$
$\dfrac{d[\beta\gamma:\alpha q_{GDP}]}{dt} = v(5) + v(9) + v(49) + v(70) - v(10)$
$\dfrac{d[GRK2^*]}{dt} = v(2) - v(3) - v(5)$
$\dfrac{d[\alpha q_{GDP}]}{dt} = v(4) + v(12) - v(5) - v(9) - v(49) - v(70)$
$\dfrac{d[pL:R]}{dt} = v(6) - v(7)$
$\dfrac{d[\alpha q_{GTP}]}{dt} = v(1) - v(4) - v(11)$
$\dfrac{d[PIP2]}{dt} = v(13) + v(72) - v(14) - v(15) - v(71)$
$\dfrac{d[IP3]}{dt} = v(15) + v(19) - v(16) - v(18)$
$\dfrac{d[DAG]}{dt} = v(15) + v(36) - v(17) - v(35)$
$\dfrac{d[IP3:ER]}{dt} = v(18) - v(19)$
$\dfrac{d[Ca]}{dt} = v(20) + v(23) - v(21) - v(22)$
$\dfrac{d[CaM:Ca]}{dt} = v(22) - v(23) - v(24) - v(59)$
$\dfrac{d[CaM:Ca:CaMK]}{dt} = v(59) - v(60)$

Ordinary Differential Equations

$$\frac{d[CaM:Ca:CN]}{dt} = v(24) - v(25)$$

$$\frac{d[pNFAT]}{dt} = v(28) + v(29) - v(26) - v(27)$$

$$\frac{d[pGSK3\beta]}{dt} = v(30) + v(31) - v(32)$$

$$\frac{d[luc(F7\_8)]}{dt} = v(33) - v(34)$$

$$\frac{d[PKC:DAG]}{dt} = v(35) - v(36)$$

$$\frac{d[IKKp]}{dt} = v(37) + v(38) - v(39)$$

$$\frac{d[I\kappa B:NF\kappa B]}{dt} = v(42) - v(43)$$

$$\frac{d[pI\kappa B:NF\kappa B]}{dt} = v(43) - v(44)$$

$$\frac{d[pI\kappa B]}{dt} = v(40) + v(44) - v(41)$$

$$\frac{d[luc(E11\_12)]}{dt} = v(45) - v(46)$$

$$\frac{d[\beta\gamma:AC]}{dt} = v(47) - v(48) - v(49)$$

$$\frac{d[PKA^*]}{dt} = v(50) - v(51)$$

$$\frac{d[pCREB]}{dt} = v(52) + v(53) - v(54) - 2*v(55)$$

$$\frac{d[pCREB:pCREB]}{dt} = v(55) - v(56)$$

$$\frac{d[luc(A11\_12)]}{dt} = v(57) - v(58)$$

$$\frac{d[pHDAC]}{dt} = v(62) + v(63) - v(64)$$

$$\frac{d[Mef2:HDAC]}{dt} = v(65) - v(61)$$

$$\frac{d[Mef2p:HDAC]}{dt} = v(61) - v(62)$$

Ordinary Differential Equations

$$\frac{d[luc(E3\_4)]}{dt} = v(66) - v(67)$$

$$\frac{d[PI3K^*]}{dt} = v(68) - v(69) - v(70)$$

$$\frac{d[PIP3]}{dt} = v(71) + v(75) + v(77) - v(72) - v(73) - v(74) - v(76)$$

$$\frac{d[Akt^*]}{dt} = v(74) - v(75)$$

$$\frac{d[BTK:PIP3]}{dt} = v(76) - v(77)$$

$$\frac{d[pATF2]}{dt} = v(78) - v(79)$$

$$\frac{d[luc(A1\_2)]}{dt} = v(80) - v(81)$$

2 Tissue-specific dose-response relationship derivation

Lisuride response in CHO cells can be described as a function of lisuride concentration (L [mol/L]) as shown in equation (S1) for the parameters given in Table S4 based on data obtained by DiscoverX dose response assay (Figure S1).

$$Response\% = Min + \frac{(Max - Min)L^n}{EC_{50}^n + L^n} \tag{S1}$$

Table S4, related to Figure 6: Agonist response parameters. Parameter values used to describe the dose-response curve in Figure S1.

Parameter	Description	Value	Units
Min	Minimum response	7.98 %	/
Max	Maximum response	36.55 %	/
EC_{50}	Effective concentration	1.076×10^{-8}	mol/L
n	Hill coefficient	0.8411	/
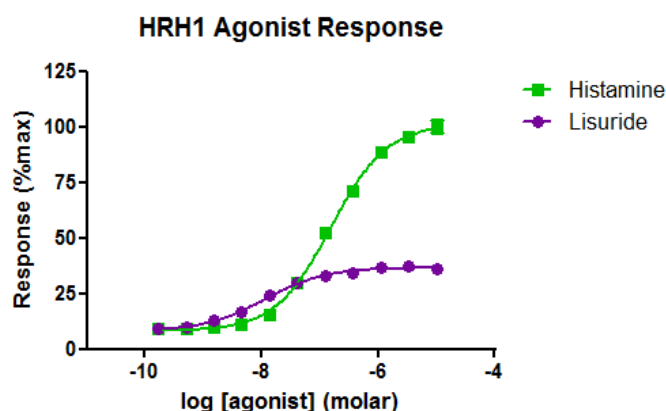
Figure S1, related to Figure 6: Ligand and agonist dose response assay. Dose response assays (DiscoverX) were used to calculate relevant EC_{50} values for both ligand (histamine) and agonist (lisuride).

2.1 *Defining the EC_{50} values for different cells and tissues*

We can describe the number of bound receptors using the equilibrium Langmuir-Hill equation:

$$R_{bound} = R_{total} \frac{L}{K_D + L}$$

where R_{total} represents the total number of receptors (bound + unbound), L represents ligand concentration and K_D is the dissociation equilibrium value.

In CHO cells, let $R_{total} = R_{total}^{CHO}$. For the ligand concentration that causes 50% maximal response (i.e. $L = EC_{50}^{CHO}$) we can derive the corresponding amount of bound receptors, $R_{bound\,50}^{CHO}$, namely:

$$R_{bound\,50}^{CHO} = R_{total}^{CHO} \frac{EC_{50}^{CHO}}{K_D + EC_{50}^{CHO}}.$$

We would expect the EC_{50} value to vary between tissues, being dependent on the relative amount of receptors in that tissue. But for simplicity we will assume that the amount of bound receptors required for a half-maximal response is the same, i.e. $R_{bound\,50}^{CHO} = R_{bound\,50}^{i}$ (for tissue i). Therefore, for tissue i we have a total number of receptors, R_{total}^{i}, and a new EC_{50} value, EC_{50}^{i} defined as below:

$$R_{bound\,50}^{i} = R_{total}^{i} \frac{EC_{50}^{i}}{K_D + EC_{50}^{i}} = R_{total}^{CHO} \frac{EC_{50}^{CHO}}{K_D + EC_{50}^{CHO}},$$

$$\Rightarrow EC_{50}^{i} = \frac{K_D EC_{50}^{CHO}}{R_{total}^{i/CHO}(K_D + EC_{50}^{CHO}) - EC_{50}^{CHO}},$$

where $R_{total}^{i/CHO} = R_{total}^{i}/R_{total}^{CHO}$. EC_{50}^{CHO} is equal to the EC_{50} found in Table S4 and using the measured K_D for lisuride, we can modify our EC50 value for each tissue and update our dose response function in equation (S1) by measuring the relative amount of receptors in tissue i compared to CHO cells, $R_{total}^{i/CHO}$.
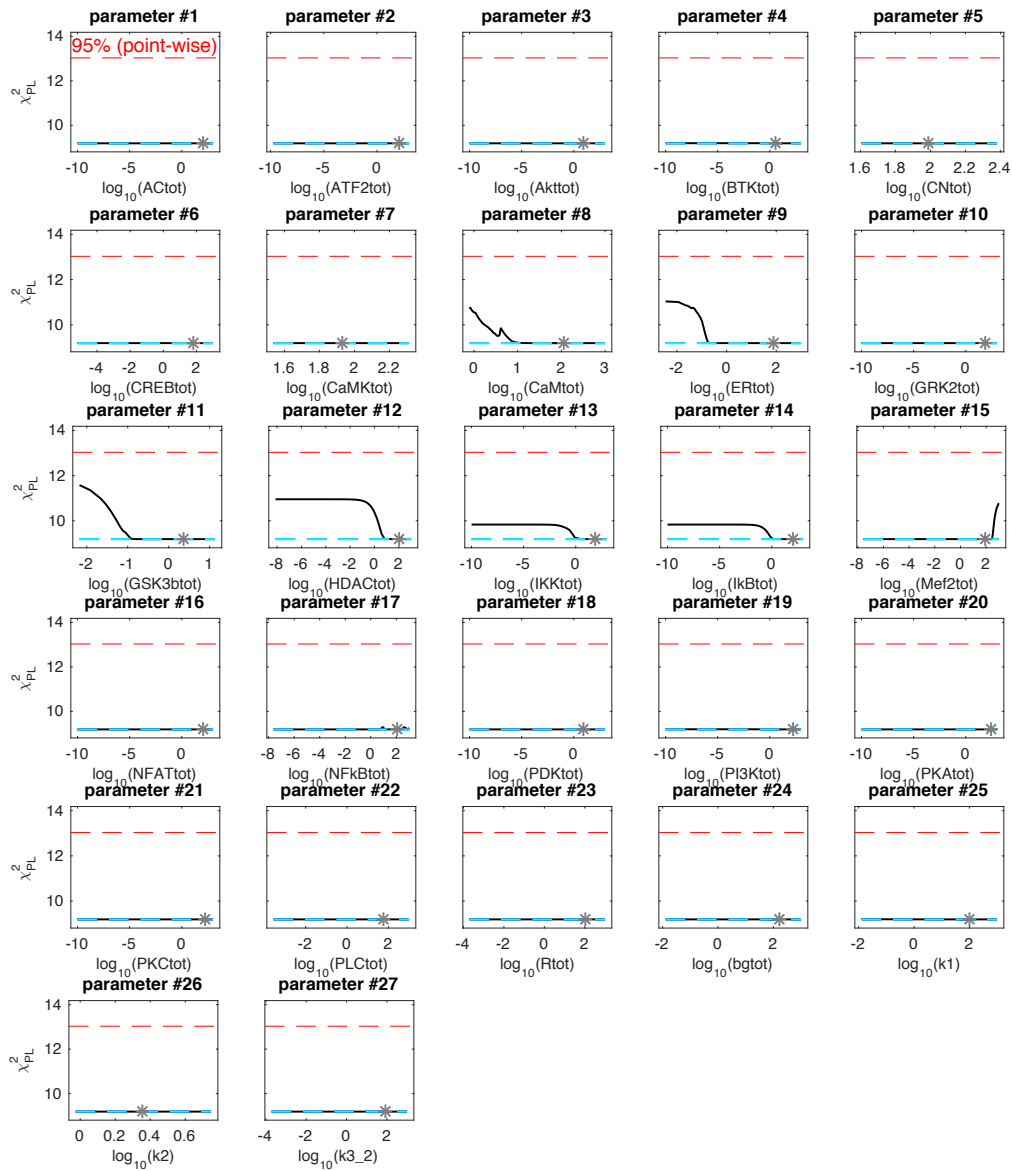
3 Identifiability Analysis

Pathway moieties were optimised to fit the steady state fold-changes of the transcription factors (Figure 2 of the main manuscript). Due to the nature of the approach taken (maximising network/pathway connectivity information rather than focusing on dynamics with a minimal model), there is an inevitable issue with model parameterisation. We have made efforts to find the global optimum for the parameter set through Latin hypercube sampling, but it is clear that other parameterisations could give fits that would at least look as good (by eye) and fit well within any expected variation from the biology/experimental error.

A profile likelihood estimation method was employed to determine parameter identifiability analysis and, as expected, the results indicate that the parameters are not uniquely identifiable for such a problem since the number of free parameters far outnumber the number of data. The analysis was performed using Data2Dynamics software (Raue et al., 2013, Raue et al., 2015) and the profile likelihood method to analyses parameter identifiability, as developed by Prof Jens Timmer's group in Freiburg (Raue et al., 2009, Maiwald et al., 2016). The results of this identifiability analysis are illustrated in Figure S2.

Additionally, local sensitivity analysis indicates that, in line with the complementary MCA method (as described in the main manuscript), it is the nodes that are relatively close to the transcription factor signal that dominate the subsequent expression following receptor activation. These fairly intuitive results suggest that errors arising due to parameter changes throughout the system can be mitigated for in order to achieve the same fold-changes seen experimentally, provided that (a) other parameters are also changed (in the case of sensitive proximal nodes) or (b) because their values are not having a large effect on the downstream signal (distal nodes). This emphasises the importance of the use of MCA in the proposed methodology as a means of identifying any distal nodes that do affect transcription factor signal, as identified in the paper. Of course, to acquire identifiable parameters, far more data would be needed (than is available for such a complex network) or typically, a minimal ODE model would be constructed that significantly reduces the number of variables and parameters that cannot be identified with given data. This minimal approach would potentially be useful for answering questions about the dynamics of the H1-histamine signalling pathway for a very specific scenario and/or ligand. However, this approach would be limited when trying to identify off-target receptor toxicity.

Figure S2, related to Figure 2: Identifiability analysis for the H1 Histamine pathway Petri net. Briefly, following the identification of a globally optimal parameter set each model parameter is perturbed within a prescribed range, one parameter at a time. Starting from the optimal value, a single parameter is perturbed, set to be fixed at the new and non-optimal value, and the model is then re-fit, i.e. by optimising all other parameters. Then corresponding likelihood values are plotted for this new fit. Analysis was conducted using the profile likelihood method in Data2Dynamics software, solved in MATLAB 2017b.

References

Heiner M, Herajy M, Liu F, Rohr C and Schwarick M (2012). Snoopy–a unifying Petri net tool. Application and Theory of Petri Nets, Springer**:** 398-407.

Hoops S, Sahle S, Gauges R, Lee C, Pahle J, Simus N, Singhal M, Xu L, Mendes P and Kummer U (2006) COPASI—a complex pathway simulator. *Bioinformatics* 22: 3067-3074.

Maiwald T, Hass H, Steiert B, Vanlier J, Engesser R, Raue A, Kipkeew F, Bock H H, Kaschek D, Kreutz C and Timmer J (2016) Driving the model to its limit: profile likelihood based model reduction. *PloS one* 11: e0162366.

Peters S A (2008) Evaluation of a generic physiologically based pharmacokinetic model for lineshape analysis. *Clinical pharmacokinetics* 47: 261-275.

Raue A, Kreutz C, Maiwald T, Bachmann J, Schilling M, Klingmüller U and Timmer J (2009) Structural and practical identifiability analysis of partially observed dynamical models by exploiting the profile likelihood. *Bioinformatics* 25: 1923-1929.

Raue A, Schilling M, Bachmann J, Matteson A, Schelke M, Kaschek D, Hug S, Kreutz C, Harms B D, Theis F J, Klingmuller U and Timmer J (2013) Lessons learned from quantitative dynamical modeling in systems biology. *PloS one* 8: e74335.

Raue A, Steiert B, Schelker M, Kreutz C, Maiwald T, Hass H, Vanlier J, Tönsing C, Adlung L, Engesser R, Mader W, Heinemann T, Hasenauer J, Schilling M, Hofer T, Klipp E, Theis F, Klingmüller U, Schoberl B and Timmer J (2015) Data2Dynamics: a modeling environment tailored to parameter estimation in dynamical systems. *Bioinformatics* 31: 3558-3560.